Met. Mater. Int., Vol. 24, No. 1 (2018), pp. 42~50
doi: 10.1007/s12540-017-7297-1

Modified Johnson-Cook Model Incorporated With Electroplasticity for Uniaxial Tension Under a Pulsed Electric Current

Moon-Jo Kim[1], Hye-Jin Jeong[2], Ju-Won Park[2], Sung-Tae Hong[3], and Heung Nam Han[2,*]

[1]Liquid processing & Casting R&D Group, Korea Institute of Industrial Technology, Incheon 21999, Republic of Korea
[2]Department of Materials Science and Engineering and Research Institute of Advanced Materials, Seoul National University, Seoul 08826, Republic of Korea
[3]School of Mechanical Engineering, University of Ulsan, Ulsan 44610, Republic of Korea

(received date: 4 May 2017 / accepted date: 29 June 2017)

An empirical expression describing the electroplastic deformation behavior is suggested based on the Johnson-Cook (JC) model by adding several functions to consider both thermal and athermal electric current effects. Tensile deformation behaviors are carried out for an AZ31 magnesium alloy and an Al-Mg-Si alloy under pulsed electric current at various current densities with a fixed duration of electric current. To describe the flow curves under electric current, a modified JC model is proposed to take the electric current effect into account. Phenomenological descriptions of the adopted parameters in the equation are made. The modified JC model suggested in the present study is capable of describing the tensile deformation behaviors under pulsed electric current reasonably well.

Keywords: alloys, deformation, mechanical properties, tensile test, electroplasticity

1. INTRODUCTION

In recent years, electrically assisted forming has been suggested as a promising new forming method, in which the mechanical property of a metal alloy can be altered by simply applying electricity to the metal alloy during deformation. Reduced flow stress and increased ductility, which are called electroplastic effects, are generally observed in electrically assisted deformation [1-3]. A number of studies have been carried out to understand the effect of electric current on mechanical behavior and microstructure of metal alloys [2-6]. According to Conrad [2], pulsed electric current directly affects the flow stress and plastic strain behavior in metals, independently of Joule heating effect. Salandro *et al.* [3] applied electric current to 5052 and 5083 aluminum alloys during uniaxial tensile testing, resulting in an increased elongation corresponding to 190% under selective pulsing conditions, compared to the elongation without electric current. Ross *et al.* [4] investigated the effect of electric current on various metal alloys including aluminum alloy, copper alloy, brass alloy, titanium alloy, and stainless steel. They reported that electric current significantly affects flow stress and elongation, regardless of microstructure or strengthening mechanism of the tested metal alloys.

Various hypotheses have been proposed to understand the mechanism of electroplastic effects. Conrad [2] suggested that the reduction of the flow stress by applying high density of electric current pulse resulted from the combined action of Joule heating and an electron wind force, which decreases the activation enthalpy for plastic deformation. Dubinko and Klepikov [7] suggested a mechanism of electroplastic deformation based on nonequilibrium fluctuations of dislocation vibrations due to the interaction between dislocations and electrons. Similar discussions based on microstructural analysis were reported by the authors [8,9], surmising that electric current plays a distinct role in annealing and aging apart from Joule heating. Other researchers argued that changes in mechanical behavior under electric current can be explained by Joule heating. Magargee *et al.* [10] applied external cooling to thin pure titanium sheet during deformation under a continuous electric current. No reduction of flow stress during the electrically assisted deformation was observed under the air-cooled condition. Therefore, the electrically assisted deformation can be described satisfactory based on thermal-mechanical constitutive models without consideration of electroplastic theory. Fan *et al.* [11] reported that Joule heating effect at grain boundaries during electrically assisted deformation affects the stress reduction in brass alloy.

Based on experimental studies on electroplasticity, efforts have been made to develop a constitutive model to account for electroplastic effects. Kronenberger *et al.* [12] developed a finite element analysis model for 6061 aluminum alloy in compression. The model accurately predicts the temperature

*Corresponding author: hnhan@snu.ac.kr

rise due to Joule heating during an electrical compression test. However, the reduction of flow stress under electric current cannot be fully demonstrated by considering only the Joule heating effect. To account for the additional effect caused by electric current, the electroplastic coefficient was introduced [13,14]. For the electrically-assisted tension [13] and bending [14] of metal alloys, closed-form solutions considering the electroplastic effect coefficient were established to describe the stress and strain relation during deformation at different electric current conditions. Recently, Roh *et al.* [15] suggested an empirical expression that describes a tensile behavior of a 5052-H32 aluminum alloy under a pulsed electric current. In a constitutive model suggested by Hariharan *et al.* [16], the electric current, which affects the mechanical behavior, was quantified by decoupling the thermal effect from the tensile behavior under a pulsed electric current. Kim *et al.* [9] also proposed a constitutive model for the flow stress responses during tensile tests under a pulsed electric current. At fixed electrical pulsing condition, annealing with precipitation hardening due to Joule heating and a distinct effect of pulsed electric current are considered simultaneously in the modified constitutive model. Although studies have been conducted on the constitutive modeling, as mentioned above, quantitative descriptions of electroplastic effects on the mechanical behavior including both annealing and aging depending on pulsing condition are still limited. In the present study, an empirical expression describing the electroplastic deformation behavior is suggested based on the Johnson-Cook (JC) model by adding several functions to take the electric current effect on hardening and thermal softening behavior into account.

2. EXPERIMENTAL PROCEDURE

The materials used in this study were commercial AZ31 (Mg-3 wt%Al-1 wt%Zn) magnesium alloy and Al-Mg-Si alloy (Al-0.87 wt%Mg-0.66 wt%Si-0.23 wt%Cu). For Al-Mg-Si alloy, specimens for tensile testing were solution heat treated at 530 °C for 1 h followed by quenching in water. After solution heat treatment, specimens were naturally aged for 4 days at room temperature. The microstructures of the AZ31 alloy and Al-Mg-Si alloy are shown in Fig. 1. For the AZ31 alloy, a strong (0001) basal fiber texture existed in the as-received sheet. The grain sizes of the AZ31 alloy and Al-Mg-Si alloy were 7 and 50 μm, respectively.

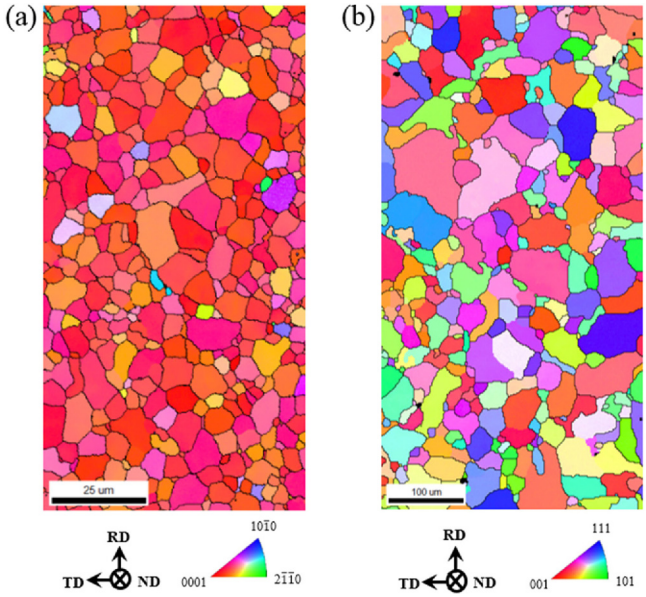

Fig. 1. Microstructure of (a) AZ31 alloy and (b) Al-Mg-Si alloy.

The experimental set-up used for quasi-static uniaxial tensile test is illustrated in Fig. 2(a) and operated at the constant crosshead speed of 1 mm/min at room temperature. The specimens used for the tensile test were prepared with a gauge width of 6.25 mm and a gauge length of 25 mm along the rolling direction according to the ASTM E8 subsize [17]. By inserting bakelite between the grips, the uniaxial tensile tester was insulated from the electric current. For the measurement of displacement during tensile testing, a non-contact measurement method type ARAMIS Digital Image Correlation (DIC) system was used. The temperature of the specimen

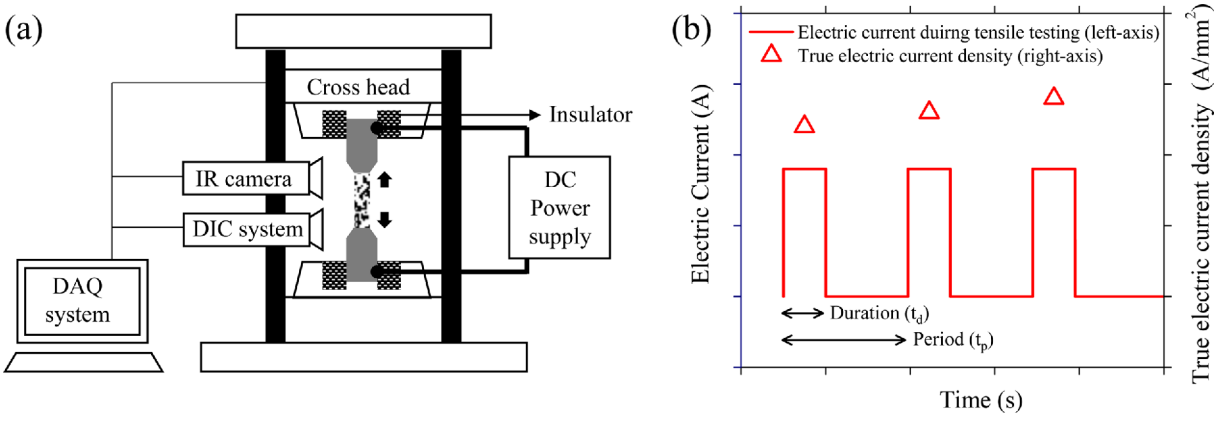

Fig. 2. (a) Instrumental set-up and (b) schematic of electric pulsing pattern during tensile testing.

during electrically-assisted tensile testing was measured using a FLIR-E40 infrared (IR) thermal imaging camera.

Electric current was generated by a Vadal SP-1000U DC power supply. A pulsed electric current with constant duration (t_d) and period (t_p) was applied to the specimen periodically until fracture (Fig. 2(b)). The amplitude of the electric current was also kept constant until fracture. As a result, the electric current density (ρ_0) based on the initial cross-sectional area of the specimen was kept constant. Note that the actual electric current density (or true electric current density) increases continuously due to the reduction of cross sectional area of the specimen during the tensile test. The electrical pulsing patterns which can result in an increase in fracture elongation without melting of material are carefully chosen in the present study. For the Al-Mg-Si alloy, pulsing patterns with ρ_0 = 60, 100, and 120 A/mm^2 under the fixed t_d = 0.5 s and t_p = 30 s were selected. The resistivity of magnesium alloy is higher than aluminum alloy. Therefore, the Joule heating is more severe in AZ31 alloy than Al-Mg-Si alloy, when the same electric current density is applied to the each material. To avoid severe Joule heating effect, lower level of electric current density (10, 30, 40, and 60 A/mm^2 with t_d = 0.5 s and t_p = 20 s) is selected in AZ31 alloy compared to Al-Mg-Si alloy.

3. RESULTS AND DISCUSSION

3.1. Mechanical behavior

The true stress-strain curves with pulsed electric current (electrically assisted tension, EA tension) compared to those without pulsed electric current (Non-EA tension) for the AZ31 alloy and the Al-Mg-Si alloy are shown in Figs. 3(a) and 3(c), respectively. For both AZ31 alloy and Al-Mg-Si alloy, the flow stress decreases nearly instantly when electric current is applied for the duration (t_d) in EA tension. The nearly instant decrease of flow stress is defined as the stress-drop and it is known as a combination of effects caused by thermal expansion due to joule heating, deceasing flow stress due to thermal softening, and electric current-induced annealing [8,15]. After the elimination of each pulse, strain hardening occurs until the next pulse of electric current. The stress-strain curve between each electric pulse is defined as the local stress-strain curve [15]. The temperature of the specimen in

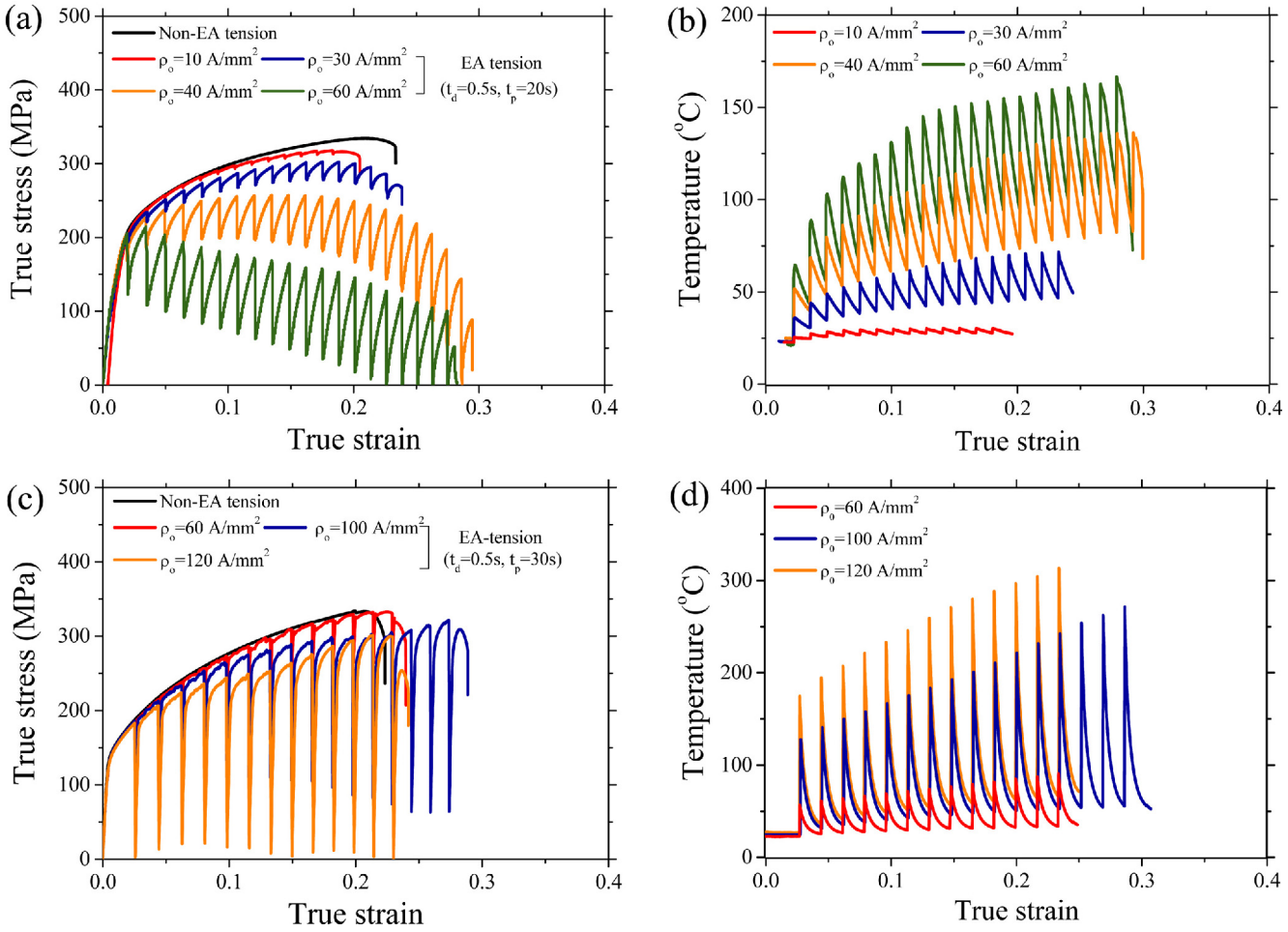

Fig. 3. (a) True stress-strain curve, (b) temperature-strain profile of AZ31 alloy and (c) true stress-strain curve, (d) temperature-strain profile of Al-Mg-Si alloy.

EA tension is shown as a function of strain for both AZ31 alloy and Al-Mg-Si alloy (Figs. 3(b) and 3(d)). The temperature increases instantly during pulsing and is decreased by air cooling until the next electrical pulse. At each maximum of the local stress-strain curve, which is called the local peak stress, the temperature of the specimen shows a local minimum due to air cooling.

For the AZ31 alloy, the flow stress of EA tension is lower than that of Non-EA tension under the given electric current condition. Also, the local peak stress in the local stress-strain curve gradually decreases as the electric current density increases at the same strain level. As discussed in open literature [8,9], the reduced flow stress in EA tension compared to Non-EA tension may be induced by the combined effect of thermal softening and electric current-induced annealing.

For the Al-Mg-Si alloy, the local peak stress in EA tension also deviates from the stress-strain curve from Non-EA tension. However, the local peak stress at $\rho_0 = 120$ A/mm^2 is almost similar to that at $\rho_0 = 100$ A/mm^2 over the strain level of 0.19. In our previous work on the Al-Mg-Si alloy, it was reported that thermal and electric current-induced precipitation hardening, i.e. aging effect, was observed with annealing under electric current. It was found that annealing affects the decrease in flow stress, while aging affects the increase in flow stress [9]. Therefore, the similar level of flow stress between $\rho_0 =$ 100 A/mm^2 and $\rho_0 = 120$ A/mm^2 over the strain level of 0.19 may be explained by the occurrence of early stage of precipitation. Note that both thermal softening and electrically induced annealing also appear to have occurred simultaneously with electrically induced aging for the Al-Mg-Si alloy as the flow stress is still lower than that of Non-EA tension for all the three electric current densities. This trend is clearly different from the trend observed for the AZ31 alloy, since AZ31 in this study is not expected to occur aging during EA tension. While it is expected that the quantity of annealing and aging under electric current depends on the electric current density, a clear quantification of the fraction of Joule heating effect and athermal electroplastic effect (electric current induced aging and annealing [8,9]) is beyond the scope of the present study, and will be reported as results of a separate study based on microstructural analysis with additional experiments.

3.2. Modified Johnson-Cook (JC) model

The original JC model is an empirical model over a wide range of strains, strain rates, and temperature [18]. It has been widely used to describe the flow stress-strain of various metal alloys [19,20]. A general equation of JC model is as follows:

$$\sigma = (A + B(\varepsilon_p)^n)(1 + \mathrm{C}\ln\dot{\varepsilon}^*)(1 - T^{*m}) \quad (1)$$

where σ is the true stress, ε_p is the equivalent plastic strain, $\dot{\varepsilon}^* = \dot{\varepsilon}/\dot{\varepsilon}_0$ is the dimensionless strain rate, $\dot{\varepsilon}$ is the true strain rate, $\dot{\varepsilon}_0$ is the reference strain rate, T^* is the homologous temperature, which is defined as $T^* = (T\text{-}T_r)/(T_m\text{-}T_r)$, T is the experimental temperature, T_r is the room temperature, and T_m is the melting temperature of the material. A, B, C, n, and m are five material constants, which are experimentally determined. The three terms of $(A+B(\varepsilon_p)^n)$, $(1+C\ln\dot{\varepsilon}^*)$, and $(1-T^{*m})$ in Eq. (1) are used to describe the work hardening effect, the strain rate effect, and the thermal softening effect, respectively. Since the elastic strain is very small compared to the plastic strain for both AZ31 alloy and Al-Mg-Si alloy, the equivalent plastic strain (ε_p) can be replaced by the true strain (ε). When strain rate is approximated as $\dot{\varepsilon} = \dot{\varepsilon}_0$, Eq. (1) can be simplified as:

$$\sigma = (A + B(\varepsilon)^n)(1 - T^{*m}) \quad (2)$$

To describe the flow stress of EA tension, a hypothetical "global stress-strain curve" is defined by connecting the local peak stress in local stress-strain curves [15]. The hypothetical global stress-strain curve can provide a simple relation to predict the macroscopic mechanical behavior without considering each local stress-strain curve in the development of electrically assisted forming in industries.

To account for the electric current effect in the global stress-strain curve, a modified JC model is suggested as:

$$\sigma = [(A + B(\varepsilon_p)^n) + (1 - \exp(D_1\varepsilon^{D_2}))](1 - T^{*m}) \quad (3)$$

where D_1 and D_2 are empirical coefficients which are functions of pulsing patterns describing the electric current effect. Since pulsing duration (t_d) and pulsing period (t_p) were set to be constant in this experiment, D_1 and D_2 are functions of electric current density (ρ_0). Note that in the present study the electric current density corresponds to the electric energy density at each pulse of electric current due to the constant pulsing duration [15]. The range of D_2 is defined as $0<D_2<1$. The relations between each D_1 and D_2 with ρ_0 are discussed in detail in sections 3.3 and 3.4.

For the EA tension, the thermal softening term of can be simply expressed as a function of strain for each pulsing pattern:

$$(1 - T^{*m}) = T_1\varepsilon^{T_2} \quad (4)$$

where T_1 and T_2 are thermal softening coefficients. Using the plot of $(1 - T^{*m})$ versus ε at each ρ_0, T_1 and T_2 can be optimized. The value of T_1 and T_2 are function of pulsing patterns, herein the function of electric current density (ρ_0) as:

$$T_1 = a\rho_0^2 + 1 \quad (5)$$

$$T_2 = b\rho_0^2 \quad (6)$$

Using the plots of T_1 and T_2 versus ρ_0, a and b are calcu-

lated. When $\rho_0 = 0$ A/mm^2, the thermal softening effect due to Joule heating and electric current effect naturally becomes negligible in the modified JC model. The modified JC model considering electric current effect finally can be written as follows:

$$\sigma = [(A + B(\varepsilon)^n) + (1 - \exp(D_1 \varepsilon^{D_2}))]((a\rho_0^2 + 1)\varepsilon^{b\rho_0^2}) \quad (0 < D_2 < 1) \tag{7}$$

3.3. Modified JC model for AZ31 alloy

The calculated true stress-strain curve of Non-EA tension for AZ31 alloy is described in Fig. 4(a) using Eq. (7) at room temperature. The material coefficients of B, ε_0, and n, are identified by optimizing the experimental data using the commercially available MATLAB software and are listed in Table 1. The calculated true stress-strain curve of Non-EA tension considering hardening effect correlates well with the experimental data. At each local peak stress of EA tension, the temperature of the specimen shows a local minimum. Based on the measured temperature at the local peak stress, the thermal softening effect, which is $1-T^{*m}$, can be calculated as a function of strain under each electric current density as shown in Fig. 4(b). The value of the thermal softening parameter m for AZ31 alloy is 1.4 [21]. T_1 and T_2 at each electric current density were plotted as shown in Figs. 4(c) and 4(d). The coefficients a and b were identified iteratively based on Eqs. (5) and (6), respectively (Table 1).

Table 1. Material constants of AZ31 alloy obtained by optimizing the experimental data

A	B	n	a	b
150	323	0.348	-3.71E-5	-9.8E-6

The predicted flow stress considering both hardening effect and thermal softening effect is always lower than that considering only hardening effect, as shown in Fig. 5. However, the local peak stress of EA tension marked by symbol in Fig. 5 is even lower than the predicted flow stress considering both hardening effect and thermal softening effect at the given electric densities in this study. As mentioned in Section 3.1, this deviation in flow stress may be explained by a combination of

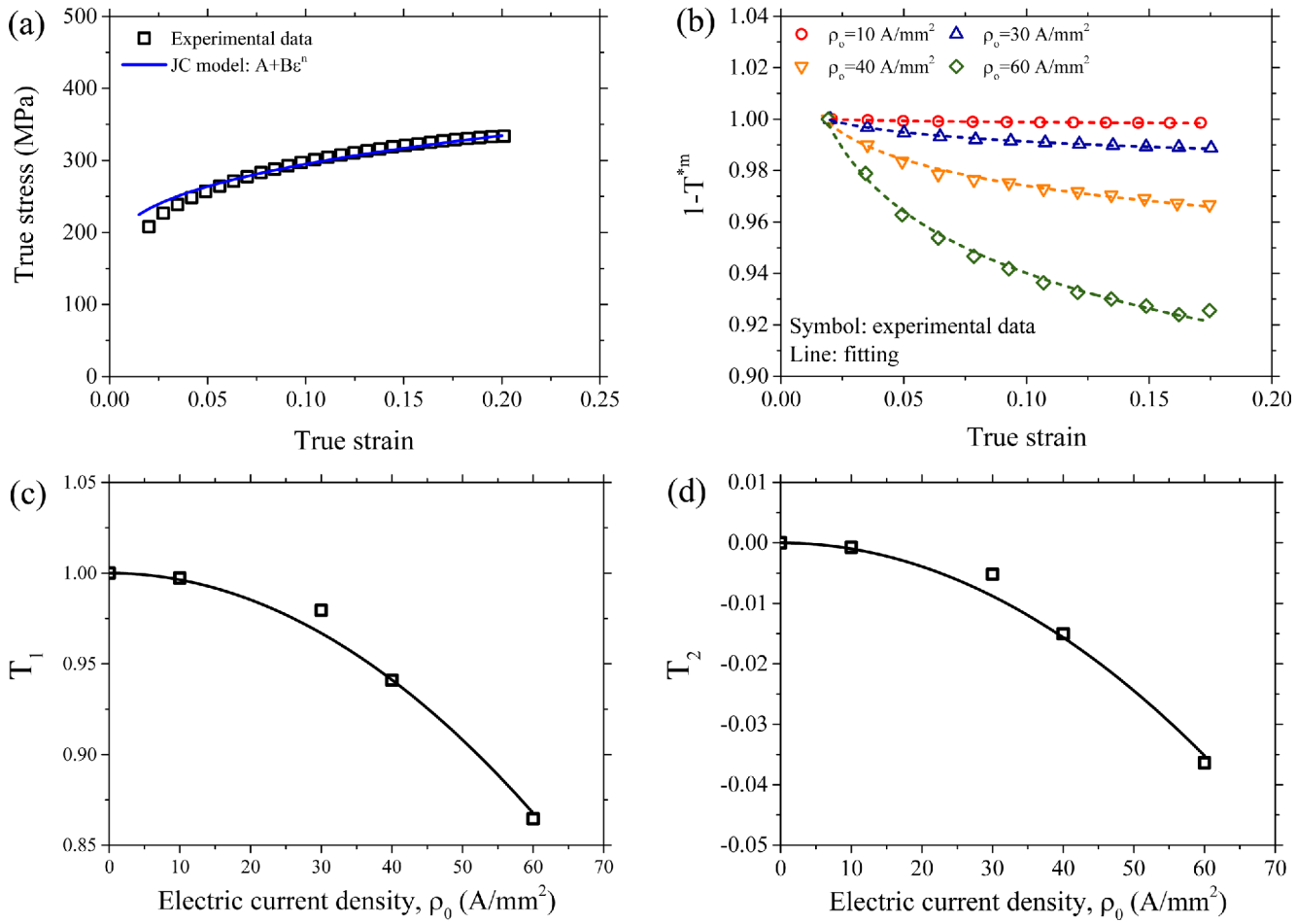

Fig. 4. (a) Experimental and Johnson-Cook fitted curves of Non-EA tension, (b) thermal softening effect at each electric current density, dependence of (c) T_1 and (d) T_2 on electric current density (ρ_0) for AZ31 alloy.

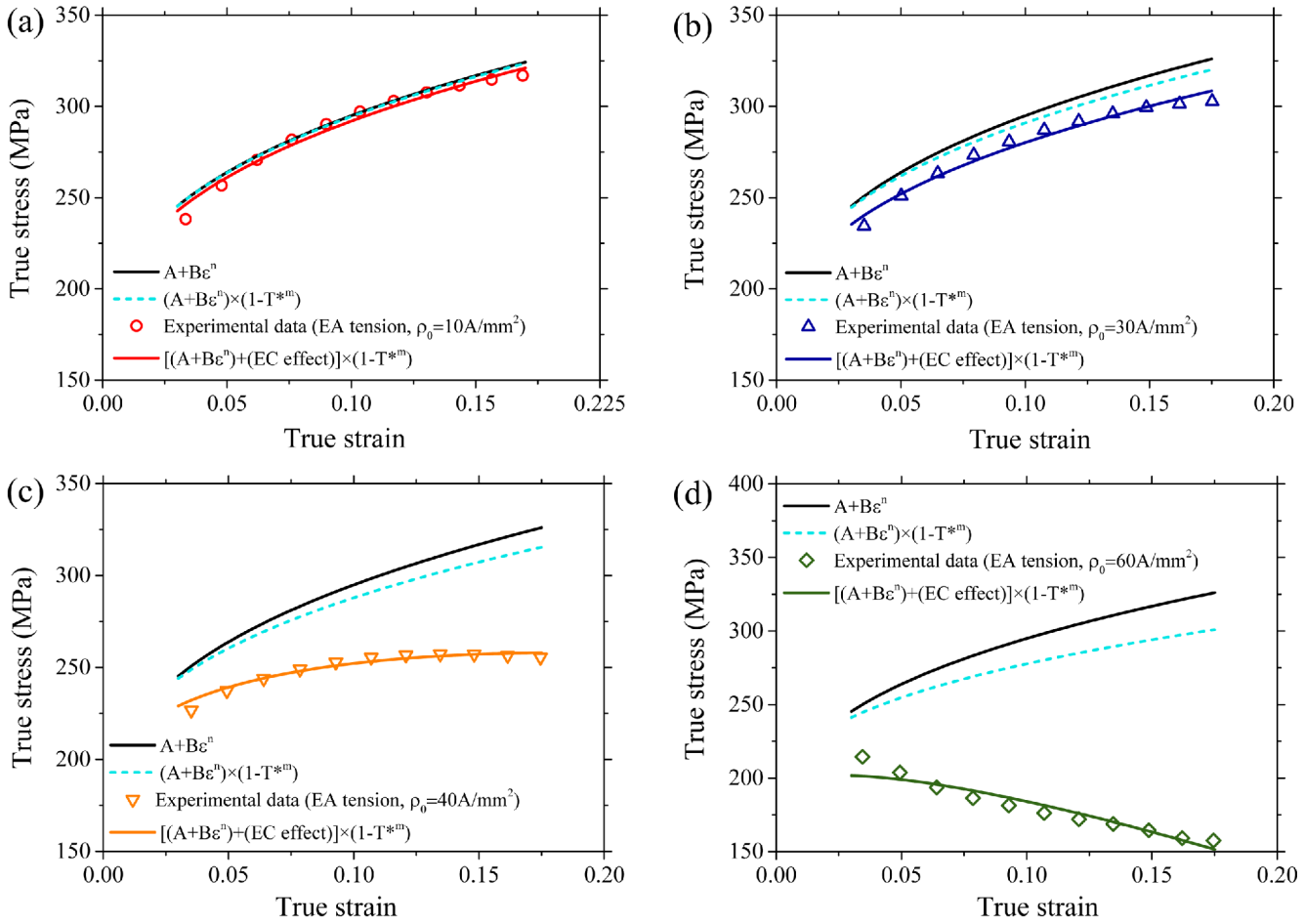

Fig. 5. Comparative plots of the experimental (symbol) and calculated (lines) flow stress from the modified JC model; (a) ρ_0 = 10 A/mm^2, (b) ρ_0 = 30 A/mm^2, (c) ρ_0 = 40 A/mm^2, and (d) ρ_0 = 60 A/mm^2 for AZ31 alloy (t_d = 0.5 s, t_p = 20 s).

accumulated Joule heating effect during previous electrical pulsing and athermal electroplastic effect, i.e. electric current-induced annealing. In the present study, electric current effect, written as EC effect in Fig. 5, includes both the accumulated thermal effect during previous electrical pulsing and athermal electroplastic effect. Using the parameter listed in Table 1, the coefficients of D_1 and D_2 in Eq. (7) are identified by optimizing the experimental data of the local peak stress in EA tension. Note that the empirical coefficients of D_1 and D_2 reflect the electric current effect, which are both thermal and athermal effects. The true stress-strain curve of EA tension calculated considering electric current effect correlates well with the experimental data as shown in Fig. 4.

In Fig. 6, the empirical coefficient of D_1 is plotted in the range of tested electric current density under EA tension. The values of D_2 are optimized as 0, 0.052, 0.22, and 0.178 at the electric current density of 10, 30, 40, and 60 A/mm^2, respectively. For AZ31 alloy, the empirical coefficient of D_1, which represents the electric current effect, gradually increases as shown in Fig. 6.

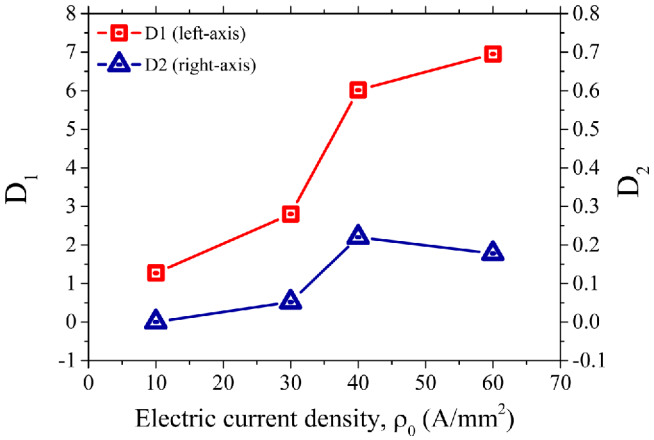

Fig. 6. Dependences of D_1 and D_2 on electric current density for AZ31 alloy.

3.4. Modified JC model for Al-Mg-Si alloy

The calculated true stress-strain curve of Non-EA tension for Al-Mg-Si alloy with experimental data is described in Fig. 7(a) using Eq. (7) at room temperature. The material coefficients A, B, ε_0, and n are identified by optimizing the experi-

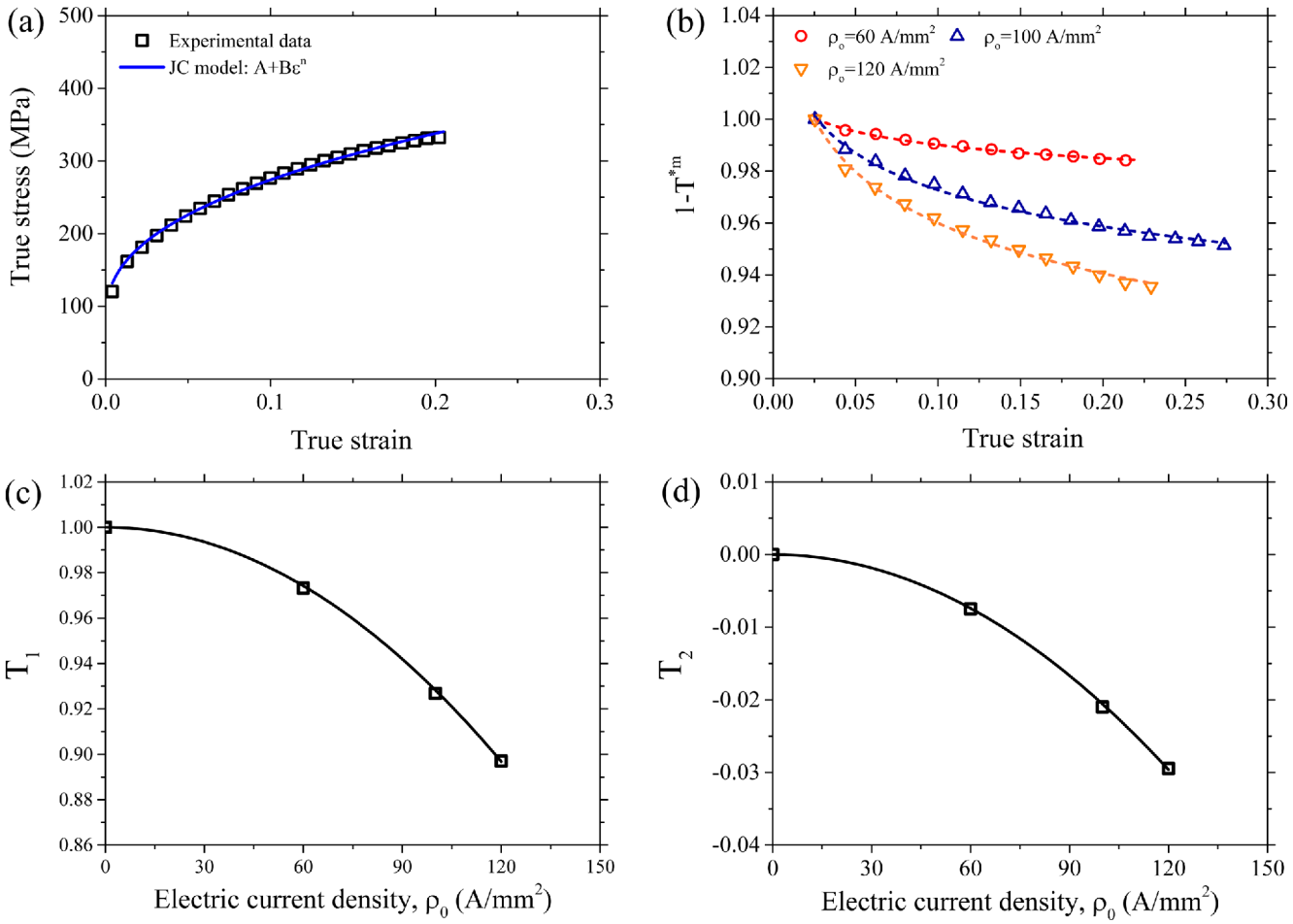

Fig. 7. (a) Experimental and Johnson-Cook fitted curves of Non-EA tension, (b) thermal softening effect at each electric current density, dependence of (c) T_1 and (d) T_2 on electric current density (ρ_0) for Al-Mg-Si alloy.

Table 2. Material constants of Al-Mg-Si alloy obtained by optimizing the experimental data

A	B	n	a	b
80	498.78	0.41	-7.17E-6	-2.06E-6

mental data in the same way used for AZ31 alloy and listed in Table 2. The thermal softening effect is also described in the same way used for AZ31 alloy (Fig. 7(b)). The value of *m* for Al-Mg-Si alloy is 1.0 [18]. The thermal softening coefficients of T_1 and T_2 were plotted as a function of electric current density (Figs. 7(c) and 7(d)), and the coefficients of *a* and *b* were identified iteratively (Table 2). Using the parameter listed in Table 2, the true stress-strain curve of EA tension is predicted by identifying the coefficients of D_1 and D_2. The true stress-strain curve of EA tension, which was calculated considering electric current effect, correlates well with the experimental data, as shown in Fig. 8.

For Al-Mg-Si alloy, the predicted flow stress, which takes both hardening effect and thermal softening effect into account, is always lower in the range of given electric current densities than that considering hardening effect only, which is similar to the result for AZ31 alloy. The local peak stress at electric current densities of 60, 100, and 120 A/mm^2 is even lower than that considering both hardening effect and thermal softening effect. These results may also be explained with electric current effect, which includes both accumulated thermal effect and athermal electric current induced annealing, as discussed for the result of AZ31 alloy.

The values of D_1 and D_2 are described in Fig. 9 as a function of electric current density. D_2 gradually decreases depending on electric current density. It is interesting to note that the value of D_1 increases at 100 A/mm^2 compared to 60 A/mm^2, while it decreases at 120 A/mm^2 compared to 100 A/mm^2. For Al-Mg-Si alloy, the values of D_1 do not gradually increase with increasing electric current density, which is different from the result for AZ31 alloy. As mentioned above, early stage of precipitation is expected to occur simultaneously with annealing during EA tension for Al-Mg-Si alloy. Therefore, we suspect that for Al-Mg-Si alloy, aging also affects the value of D_1 in addition to

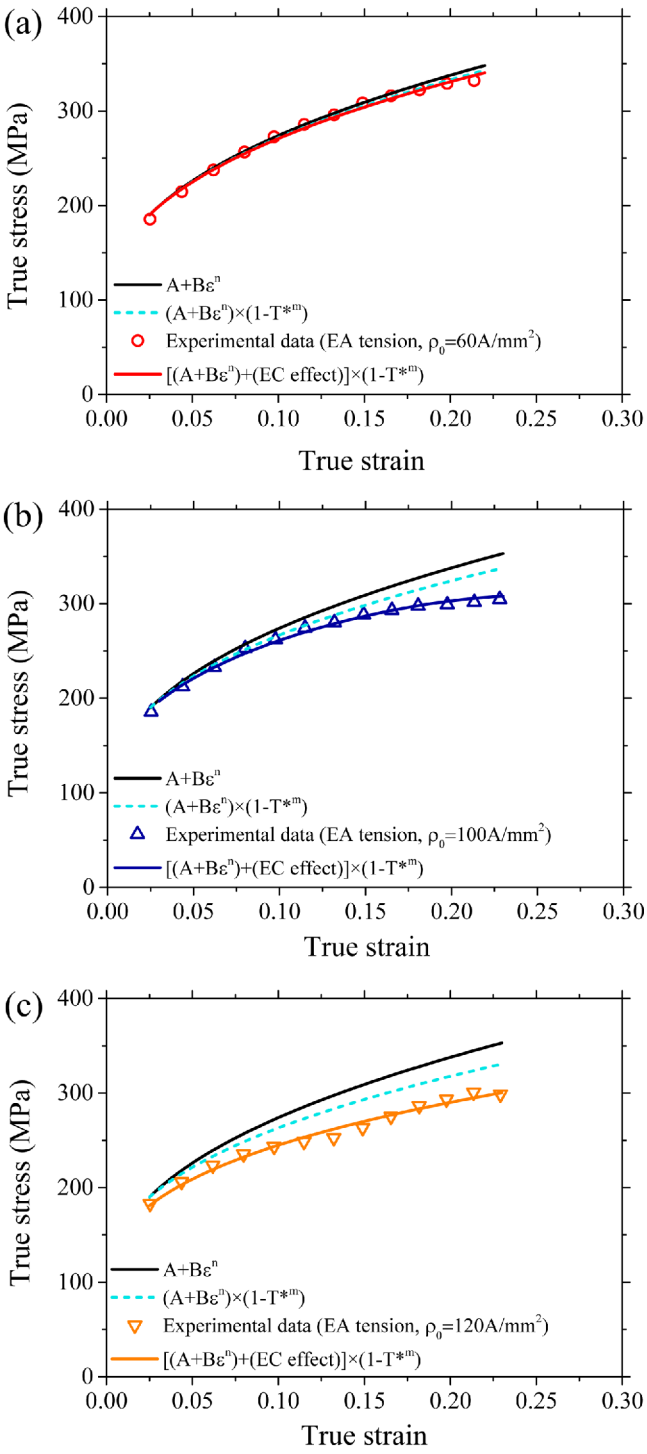

Fig. 8. Comparative plots of the experimental (symbol) and calculated (lines) flow stress from the modified JC model; (a) $\rho_0 = 60$ A/mm^2, (b) $\rho_0 = 100$ A/mm^2, and (c) $\rho_0 = 120$ A/mm^2 for Al-Mg-Si alloy ($t_d = 0.5$ s, $t_p = 30$ s).

the annealing under pulsed electric current. Future investigations on the contribution of electric current to aging and annealing effect will enable accurate quantification of the coefficient D_1.

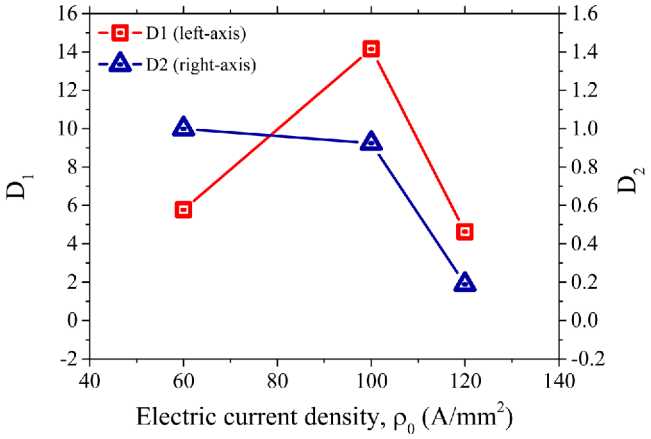

Fig. 9. Dependences of D_1 and D_2 on electric current density for Al-Mg-Si alloy.

4. CONCLUSION

An empirical expression describing the electroplastic deformation behavior is suggested based on the Johnson-Cook (JC) model by adding several functions to take into account electric current effect with hardening and thermal softening behavior. The mechanical behaviors of AZ31 alloy and Al-Mg-Si alloy were investigated under pulsed electric current at various electric current densities with a fixed duration of electric current. The upper boundary of the stress-strain curve in EA tension described by the modified JC model is compared to the experimental results of EA tension. Phenomenological descriptions of coefficients to describing the electric current effect are demonstrated as a function of electric current density. Annealing and aging by applying electric current also affect the empirical coefficient of D_1. However, the contribution of electric current to annealing and aging effect on the coefficient D_1, which has a physical meaning, is not quantified in the present study. The modified JC model suggested in the present study is capable of describing the experimental results reasonably well.

ACKNOWLEDGEMENT

This work was supported by the National Research Foundation of Korea (NRF) grant funded by the Korea government (MSIP; Ministry of Science, ICT & Future Planning) (No.2017R1C1B2012459) and the Engineering Research Center (ERC) program of the National Research Foundation of Korea (NRF) grant funded by the Ministry of Science, ICT & Future Planning (MSIP) (NO. NRF-2015R1A5A1037627). STH was supported by the Technology Innovation Program (Industrial strategic technology development program, 10044807. Development of technologies for vehicle body part made from UHSS and Al5000 by electrically assisted manufacturing) funded by the Ministry of Trade, Industry & Energy (MOTIE, Korea).

REFERENCES

1. O. A. Troitskii, *Pisma Zh. Tekh. Fiz.* **10**, 18 (1969).
2. H. Conrad, *Mat. Sci. Eng. A* **287**, 276 (2000).
3. W. A. Salandro, J. J. Jones, T. A. McNeal, J. T. Roth, S.-T. Hong, and M. T. Smith, *J. Manuf. Sci. E.-Trans. ASME* **132**, 051016 (2010).
4. C. D. Ross, D. B. Irvin, and J. T. Roth, *J. Eng. Mater. Technol.* **129**, 342 (2007).
5. S.-T. Hong, Y.-H. Jeong, N. Chowdhury, D.-M. Chun, M.-J. Kim, and H. N. Han, *CIRP Ann.-Manuf. Techn.* **64**, 277 (2015).
6. W. Kim, K.-H. Yeom, N. T. Thien, S.-T. Hong, B.-K. Min, S. I. Oh, *et al. CIRP Ann.-Manuf. Techn.* **63**, 273 (2014).
7. V. I. Dubinko and V. F. Klepikov, *Bull. Russ. Acad. Sci. Phys.* **72**, 1188 (2008).
8. M.-J. Kim, K. Lee, K. H. Oh, I.-S. Choi, S.-T. Hong, H. N. Han, *et al. Scripta Mater.* **75**, 58 (2014).
9. M.-J. Kim, M.-G. Lee, K. Hariharan, S.-T. Hong, I.-S. Choi, H. N. Han, *et al. Int. J. Plasticity* **94**, 148 (2017).
10. J. Magargee, F. Morestin, and J. Cao, *J. Eng. Mater. Technol.* **135**, 041003 (2013).
11. R. Fan, J. Magargee, P. Hu, and J. Cao, *Mat. Sci. Eng. A* **574**, 218 (2013).
12. T. J. Kronenberger, D. H. Johnson, and J. T. Roth, *J. Manuf. Sci. Eng.* **131**, 031003 (2009).
13. C. Bunget, W. A. Salandro, L. Mears, and J. T. Roth, *Trans. N. Amer. Manufac.* **38**, 647 (2010).
14. W. A. Salandro, C. Bunget, and L. Mears, *J. Manuf. Sci. E.-Trans. ASME* **133**, 041008 (2011).
15. J.-H. Roh, J.-J. Seo, S.-T. Hong, M.-J. Kim, and H. N. Han, *Int. J. Plasticity* **58**, 84 (2014).
16. K. Hariharan, M.-G. Lee, M.-J. Kim, H. N. Han, D. Kim, and S. Choi, *Metall. Mater. Trans. A* **46**, 3043 (2015).
17. Standard E8/E8M-09, *Standard Test Methods for Tension Testing of Metallic Materials*, ASTM International, USA (2011).
18. G. R. Johnson and W. H. Cook, *Proc. Seventh International Symposium on Ballistic*, pp.541-547, The Hague, Netherlands (1983).
19. Y. Hu, Y. X. Jin, H. Zheng, Y. Zhou, and J. Shao, *Met. Mater. Int.* **22**, 1015 (2016).
20. J. Zhao, Z. Jiang, G. Zu, W. Du, X. Zhang, and L. Jiang, *Met. Mater. Int.* **22**, 474 (2016).
21. I. Ulaciaa, C. P. Salisbury, I. Hurtado, and M. J. Worswick, *J. Mater. Proc. Technol.* **211**, 830 (2011).